

Determination of dielectric properties of titanium carbide fabricated by microwave synthesis with Ti-bearing blast furnace slag

Peng Liu, Li-bo Zhang, Bing-guo Liu, Guang-jun He, Jin-hui Peng, and Meng-yang Huang

Cite this article as:

Peng Liu, Li-bo Zhang, Bing-guo Liu, Guang-jun He, Jin-hui Peng, and Meng-yang Huang, Determination of dielectric properties of titanium carbide fabricated by microwave synthesis with Ti-bearing blast furnace slag, *Int. J. Miner. Metall. Mater.*, 28(2021), No. 1, pp. 88-97. <https://doi.org/10.1007/s12613-020-1985-4>

View the article online at [SpringerLink](#) or [IJMMM Webpage](#).

Articles you may be interested in

Hong-rui Yue, Tao Jiang, Qiao-yi Zhang, Pei-ning Duan, and Xiang-xin Xue, [Electrorheological effect of Ti-bearing blast furnace slag with different TiC contents at 1500](#), *Int. J. Miner. Metall. Mater.*, 24(2017), No. 7, pp. 768-775. <https://doi.org/10.1007/s12613-017-1460-z>

Chang-hong Chen, Ke-qin Feng, Yu Zhou, and Hong-ling Zhou, [Effect of sintering temperature on the microstructure and properties of foamed glass-ceramics prepared from high-titanium blast furnace slag and waste glass](#), *Int. J. Miner. Metall. Mater.*, 24(2017), No. 8, pp. 931-936. <https://doi.org/10.1007/s12613-017-1480-8>

Amir Karimzadeh Behnami, Arman Hoseinpur, Masoud Sakaki, Mohammad Sh. Bafghi, and Kazumichi Yanagisawa, [Synthesis of WC powder through microwave heating of WO₃-C mixture](#), *Int. J. Miner. Metall. Mater.*, 24(2017), No. 2, pp. 202-207. <https://doi.org/10.1007/s12613-017-1396-3>

Mustafa K. Ibrahim, E. Hamzah, Safaa N. Saud, E. N. E. Abu Bakar, and A. Bahador, [Microwave sintering effects on the microstructure and mechanical properties of Ti-51at%Ni shape memory alloys](#), *Int. J. Miner. Metall. Mater.*, 24(2017), No. 3, pp. 280-288. <https://doi.org/10.1007/s12613-017-1406-5>

Hong-ling Zhou, Ke-qin Feng, Chang-hong Chen, and Zi-di Yan, [Influence of CeO₂ addition on the preparation of foamed glass-ceramics from high-titanium blast furnace slag](#), *Int. J. Miner. Metall. Mater.*, 25(2018), No. 6, pp. 689-695. <https://doi.org/10.1007/s12613-018-1616-5>

Yan-xiang Liu, Jian-liang Zhang, Zhi-yu Wang, Ke-xin Jiao, Guo-hua Zhang, and Kuo-chih Chou, [Dripping and evolution behavior of primary slag bearing TiO₂ through the coke packed bed in a blast-furnace hearth](#), *Int. J. Miner. Metall. Mater.*, 24(2017), No. 2, pp. 130-138. <https://doi.org/10.1007/s12613-017-1387-4>



IJMMM WeChat



QQ author group

Determination of dielectric properties of titanium carbide fabricated by microwave synthesis with Ti-bearing blast furnace slag

Peng Liu^{1,2,3,4}, Li-bo Zhang^{1,2,3,4}, Bing-guo Liu^{1,2,3,4}, Guang-jun He^{1,2,3,4,5}, Jin-hui Peng^{1,2,3,4}, and Meng-yang Huang⁶

1) State Key Laboratory of Complex Nonferrous Metal Resources Clean Utilization, Kunming University of Science and Technology, Kunming 650093, China

2) Yunnan Provincial Key Laboratory of Intensification Metallurgy, Kunming 650093, China

3) National Local Joint Laboratory of Engineering Application of Microwave Energy and Equipment Technology, Kunming 650093, China

4) Faculty of Metallurgical and Energy Engineering, Kunming University of Science and Technology, Kunming 650093, China

5) Faculty of Science, Kunming University of Science and Technology, Kunming 650500, China

6) Yunnan Energy Research Institute Co., Ltd., Kunming 650093, China

(Received: 24 October 2019; revised: 8 January 2020; accepted: 9 January 2020)

Abstract: The preparation of functional material titanium carbide by the carbothermal reduction of Ti-bearing blast furnace slag with microwave heating is an effective method for valuable metals recovery; it can alleviate the environmental pressure caused by slag stocking. The dynamic dielectric parameters of Ti-bearing blast furnace slag/pulverized coal mixture under high-temperature heating are measured by the cylindrical resonant cavity perturbation method. Combining the transient dipole and large π bond delocalization polarization phenomena, the interaction mechanism of the microwave macroscopic non-thermal effect on the titanium carbide synthesis reaction was revealed. The material thickness range during microwave heating was optimized by the joint analysis of penetration depth and reflection loss, which is of great significance to the design of the microwave reactor for the carbothermal reduction of Ti-bearing blast furnace slag.

Keywords: titanium-bearing blast furnace slag; dielectric mechanism; penetration depth; reflection loss; microwave heating; efficiency

1. Introduction

Titanomagnetite is a complex iron ore [1–2] mainly concentrated in Russia, China, South Africa, and the United States. In China, Panzhihua titanomagnetite reserves are about 9.66 billion tons [3–5], and the titanium and vanadium deposits account for 35.17wt% and 11.6wt% of the world's total reserves, respectively. At present, the main way to utilize titanomagnetite is the blast furnace smelting process [6]. Pelletizing concentrate is smelted by a blast furnace to produce hot metal and about 600000 t of Ti-bearing (22wt%–25wt%) blast furnace slag every year [7–8]. The blast furnace slag composition is complex and the titanium oxide phase distribution is dispersive. With the existing technology, blast furnace slag can be used as building materials, but this will cause a waste of titanium resources. Rutile or dye-grade titanium dioxide (TiO₂) can also be prepared by the wet process [9–10], but the demand for the corresponding products is limited; therefore, exploring new processes

for the utilization of blast furnace slag resources is necessary [11–12].

According to the microwave absorbing property [13–14], this paper presents the idea of preparing titanium carbide by microwave heating with blast furnace slag/pulverized coal mixture as raw material; this method enables to reduce energy consumption as much as possible while resolving the environmental problems and resource waste caused by the accumulation of blast furnace slag. Many studies have shown that TiC, as a structural ceramic, has a unique structure and many ideal properties [15–17], such as high melting point, good thermal conductivity, chemical stability, electrical conductivity, and excellent mechanical properties. Therefore, TiC is widely used in the fabrication of cutting tools, pumps, electrodes, inductive materials, thermocouples, and other functional devices. The study on the dielectric properties of blast furnace slag shows that its absorbing effect is acceptable. In addition, carbon in pulverized coal can also be heated rapidly in the microwave field [18]. Therefore, TiC preparation by

Corresponding authors: Bing-guo Liu E-mail: bingoliu@126.com; Guang-jun He E-mail: hegj9@126.com

© University of Science and Technology Beijing and Springer-Verlag GmbH Germany, part of Springer Nature 2020

carbothermal reduction in a microwave field with blast furnace slag/pulverized coal mixture is a feasible technology for effectively utilizing titanium resources and alleviating the environmental pressure caused by slag accumulation.

Compared with the traditional heating method (Table 1), microwave heating has the characteristics of selective and outward-oriented temperature gradient, and has non-thermal effects on reactions during heating [19–20]. The non-thermal effects of the interaction between the microwave and the material can be divided into two categories: the subatomic non-thermal effect (S-NTE) and the macroscopic non-thermal effect (M-NTE). Generally, non-thermal effects promote the reactions. It has been reported that the quantum tunneling effect of the electronic state is the cause of the S-NTE; that is, the bonding electrons in the microwave field can pass through the energy barrier by means of quantum effect under low-energy conditions to realize the state transition [21]. For

M-NTE, this work first discusses the mechanism of titanium carbide microwave synthesis reaction from the perspective of transient dipoles. On this basis, non-loss energy storage phenomenon (delocalized dipole) caused by the M-NTE when microwave is applied to the carbon material is analyzed to explain the M-NTE promotion of the corresponding chemical reactions. In addition, based on the high-temperature dynamic dielectric parameter testing technology, the penetration depth theory and the reflection loss theory are combined to optimize the material thickness in the microwave field to improve the microwave energy utilization efficiency. This parameter can be applied to the design of industrial-grade microwave reactors to treat Ti-bearing slag. Finally, a process flow chart of the microwave synthesis of titanium carbide from titanium blast furnace slag/pulverized coal mixture is proposed, which can combine microwave heating and solid waste resource recovery technologies.

Table 1. Features of microwave and conventional heating

Heating method	Energy conversion	Heat transfer	Heating characteristic	$-\Delta T$	Non-thermal effect
Conventional	$E_T \xrightarrow{\eta_C} E_H$	Major role	 Non-selective	 Out→Inner	×
Microwave	$E_E \xrightarrow{\eta_{M1}} E_M \xrightarrow{\eta_{M2}} E_H$	Associated	 Selective	 Inner→Out	√

Note: $-\Delta T$ —Decreasing direction of temperature gradient; E_T —Total Energy; E_E —Electric Energy; E_H —Heat in material; E_M —Microwave energy; η_C , η_{M1} , and η_{M2} —Energy efficiencies in conventional heating and the first and second steps in microwave heating method, respectively; ×—There is no non-thermal effect in the heating process; √—Non-thermal effect is accompanied by the heating process.

2. Experimental

2.1. Materials

The phase composition of Ti-bearing blast furnace slag (from Panzhihua Iron & Steel (Group) Co., China) powder is listed in Table 2. The mass percentages of Ca, Si, Ti, and Al oxides account for about 90%, while those of Mg and Fe oxides account for about 10%. Anthracite (>200 meshes) was used as a reductant, and the carbon content was 92wt%. X-ray powder diffraction (XRD, X’Pert³ Powder, PANalytical, Cu K α radiation) in Fig. 1(a) and scanning electron microscopy (SEM, Type: Phenom proX; Brand: Phenom) analyses (Fig. 1(b), Table 3) of the Ti-bearing blast furnace slag show that the main phase can be divided into two: a high silicon phase and a high titanium phase. The high silica phase is fassaite ((Ca_xMg_yFe_zAl_uTi_{1.985-x-y-z-u})(Si₁Al_{2-v})O₆), and the high titanium phase is perovskite (Ca(TiO₃)). The SEM mapping (Fig. 2(a)) and corresponding energy-dispersive X-ray spec-

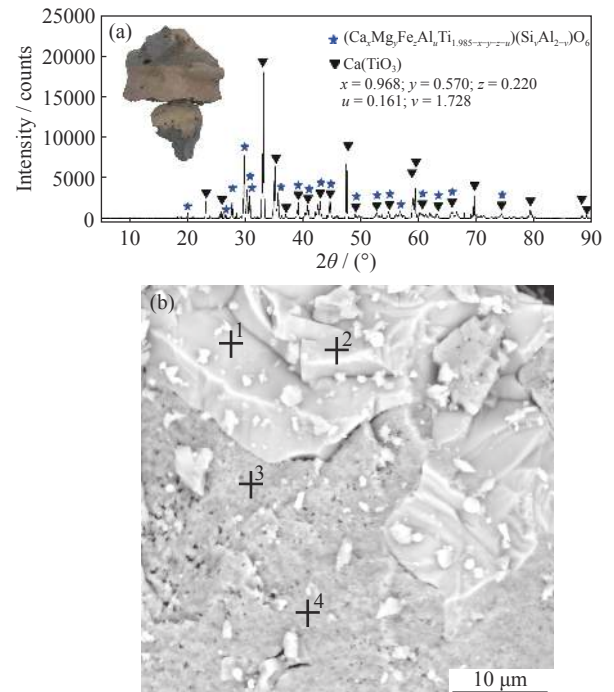


Fig. 1. (a) XRD pattern and (b) SEM micrograph of Ti-bearing blast furnace slag. Inset in (a) is the block of Ti-bearing blast furnace slag.

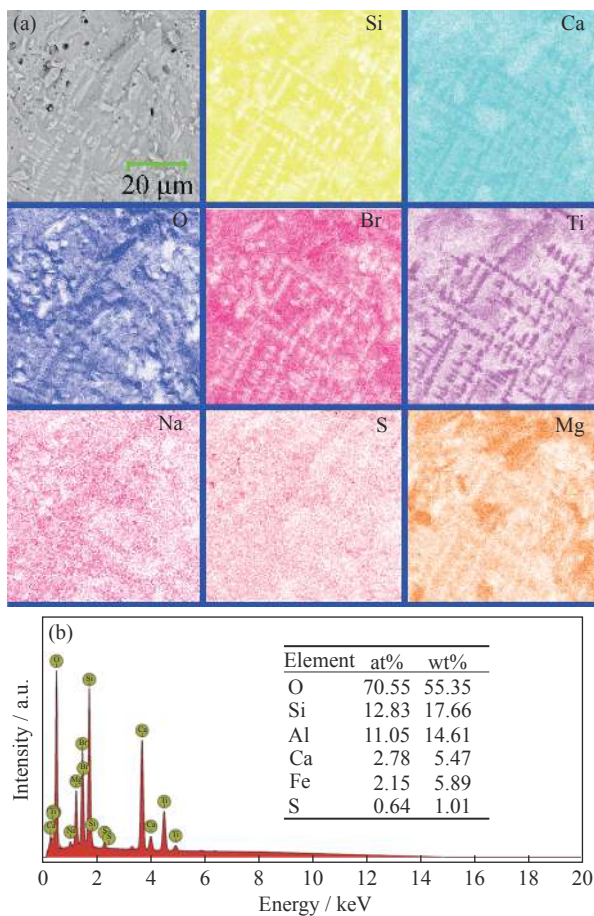
Table 2. Composition of Ti-bearing blast furnace slag wt%

CaO	SiO ₂	TiO ₂	Al ₂ O ₃	MgO	Fe ₂ O ₃
29.08	24.52	22.18	13.61	6.41	3.60

Table 3. Energy-dispersive X-ray spectroscopy (EDS) analyses for points 1–4 in Fig. 1(b)

Point	O		Ca		Ti		Si		Br		Al		Mg		Mn		S	
	at%	wt%	at%	wt%	at%	wt%	at%	wt%	at%	wt%	at%	wt%	at%	wt%	at%	wt%	at%	wt%
1	59.89	35.04	19.46	28.53	18.73	32.79	1.04	1.07	0.88	2.57	—	—	—	—	—	—	—	—
2	80.04	59.68	9.78	18.26	9.51	21.22	—	—	0.88	2.57	0.67	0.84	—	—	—	—	—	—
3	58.55	34.69	15.24	22.62	6.42	11.38	9.71	10.10	4.71	13.94	—	—	3.54	3.19	0.72	1.46	0.67	0.80
4	66.70	43.69	7.66	12.56	3.70	7.24	10.81	12.43	5.54	18.12	—	—	4.40	4.38	—	—	1.20	1.58

troscopy (EDS) analysis (Fig. 2(b)) of the flat region show the dispersive distribution and fishbone morphology of titanium oxide in the blast furnace slag. This is also the main reason for the difficulty in recycling titanium-containing blast furnace slag resources.

**Fig. 2. (a) SEM mapping and (b) EDS analysis of the flat area of the titanium-bearing blast furnace slag.**

Ti-bearing blast furnace slag was ground into powder (>200 meshes) and mixed with anthracite at a mass ratio of 1:1 to prepare the dynamic dielectric test sample and microwave synthesis sample.

2.2. Measurement and microwave heating

2.2.1. Dielectric parameter measurement

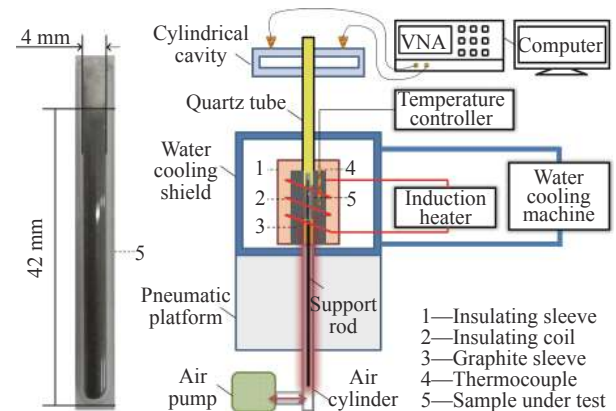
The real part of complex permittivity can describe microwave energy storage capacity in the area where the mater-

ial is located, while the imaginary part describes the interaction strength of materials with microwave in the form of damping and conductive loss (Eq. (1)).

$$\varepsilon = \varepsilon_0 \varepsilon_r = \varepsilon_0 (\varepsilon_r' - i \varepsilon_r'') \quad (1)$$

where ε is the complex permittivity (F/m), ε_0 is vacuum permittivity (8.854×10^{-12} F/m), ε_r is the relative complex permittivity, ε_r' is the relative dielectric constant, ε_r'' is the relative dielectric loss, and i is the imaginary unit.

The cylindrical resonator perturbation method is used for the dielectric parameter measurement in this study [22–23]. The resonant frequency of the resonator is 2450 MHz. The structure of the dielectric parameter testing equipment with the sample tube is shown in Fig. 3. The sample (in a little bottom-end sealed quartz tube) can slide in the quartz pipe through the air pump switch. During the test, the sample rose to the cylindrical resonator. After testing at a certain temperature, the sample dropped to the heating area to be heated. The relative dielectric constant and dielectric loss of the sample at different temperatures were measured during the reaction without cooling down.

**Fig. 3. Schematic graph of the apparatus used to perform high-temperature complex permittivity measurement (VNA—Vector network analyzer).**

Calibration experiments with air and water as reference materials were conducted to ensure the test accuracy. As shown in Table 4, air is a low-loss material, the measured data of ε_r' (air) is close to the reference data [24], and nearly equal to 1; the measured data of ε_r'' (air) is nearly equal to 0; while water is a high-loss material, the measured data of ε_r' (water) is close to the two reference data [25–26]; the measured data of ε_r'' (water) is between the two reference data

(9.40 and 18.77). Therefore, the equipment can accurately measure the dielectric range from air to water, which covers the dielectric test range of the materials involved in this study.

Table 4. Calibration results of the dielectric testing system in Fig. 3 (2450 MHz, 25°C)

Material	ϵ_r'	ϵ_r''	Ref.
Air	1.00059	—	[24]
	1.00043	0.00085	This work
Water	78.32	18.77	[25]
	76.66	9.40	[26]
	78.19	15.38	This work

2.2.2. Microwave synthesis and thermodynamics

From thermodynamics analysis (Fig. 4), when titanium oxide reacts with carbon alone (Eq. (2)), the synthesis reaction may occur at a temperature of 1289°C, which is higher than the reaction temperature of 1003°C when iron oxide is exited at the same time (Eq. (3)). This indicates that the iron oxide is beneficial to the TiC synthesis [2,4]. In addition, gas-based reduction (CO) [27] is beneficial to the separation of TiO₂ from FeTi₂O₅ in Eq. (3).

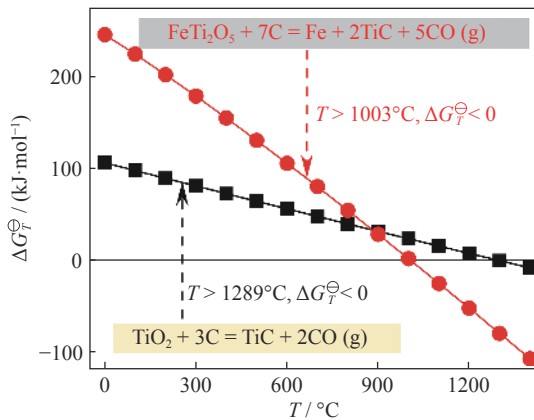
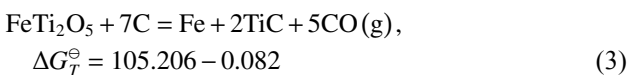
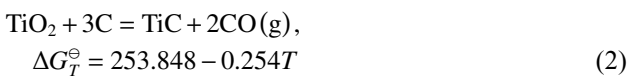


Fig. 4. Standard Gibbs free energy (ΔG_T^\ominus) vs. temperature (T) curves for TiO₂ and FeTi₂O₅.



where ΔG_T^\ominus is standard Gibbs free energy (kJ/mol), T is the temperature. The mass ratios of carbon to oxygen are 31.08:68.92 and 26.63:73.37 for Eqs. (2) and (3), respectively. Due to the influence of the reaction kinetics factors, the actual temperatures of the reactions are usually higher than the thermodynamically calculated temperatures.

The device for the microwave carbothermal synthesis of titanium carbide with the sample is shown in Fig. 5. It is mainly composed of a heating chamber, microwave generat-

ing device (2450 MHz), and temperature control system. The power of the microwave furnace is continuously adjustable from 0–3000 W, enabling automatic temperature control. Corundum, a wave-transparent material, was used for the crucible because of its low dielectric parameter. Moreover, the sample (100 g) was placed in the crucible, at the center of the reaction cavity bottom. During the microwave heating process, the sample temperature was controlled to 1200°C by a K-type thermocouple, and this state was maintained for 30 min. After the reaction, the material was characterized by SEM, and the reaction mechanism was analyzed from a dielectric aspect. Afterward, XRD analyses of the mixture at different temperatures (500°C/700°C/900°C/1100°C/1150°C/1200°C) were conducted to confirm the TiC phase transformation.

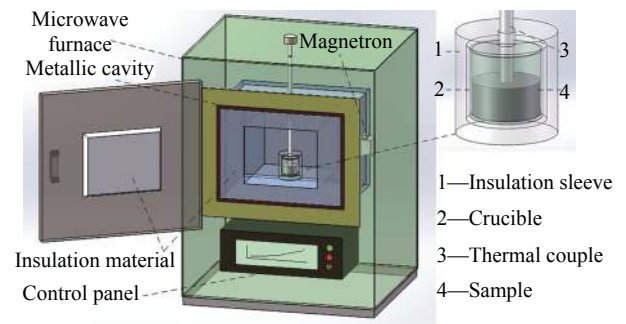


Fig. 5. Microwave heating furnace in lab-scale (crucible inner sizes: $\phi 50$ mm; height of 60 mm; wall thickness of 5 mm).

3. Results and discussion

3.1. Dielectric analysis and phase transformation

The results of dielectric parameters measurement are shown in Fig. 6(a). The figure can be divided into four regions according to the changing trend. The loss tangent ($\tan\delta$) is a derived parameter from the parameters of ϵ_r' and ϵ_r'' as shown in Eq. (4), which is used to describe the ratio of active power to reactive power. The loss tangent also describes the ratio of loss energy to action energy in the volume range of the microwave heating sample [28].

$$\tan\delta = \frac{\epsilon_r''}{\epsilon_r'} \quad (4)$$

The trend of loss tangent (Fig. 6(b)) confirms the correctness of regional division. The regional scatter shapes comprise two reaction stages in Fig. 6(a) and two reaction peaks in Fig. 6(b).

Dielectric parameters in the flat region (25–700°C) are stable, reflecting the difficult treatment of Ti-bearing slag. A small-scale reaction, related to the combustion or volatilization of some combustibles in pulverized coal, took place at the first critical point (700–900°C), which caused the fluctuation of the dielectric parameters. After the reaction, the

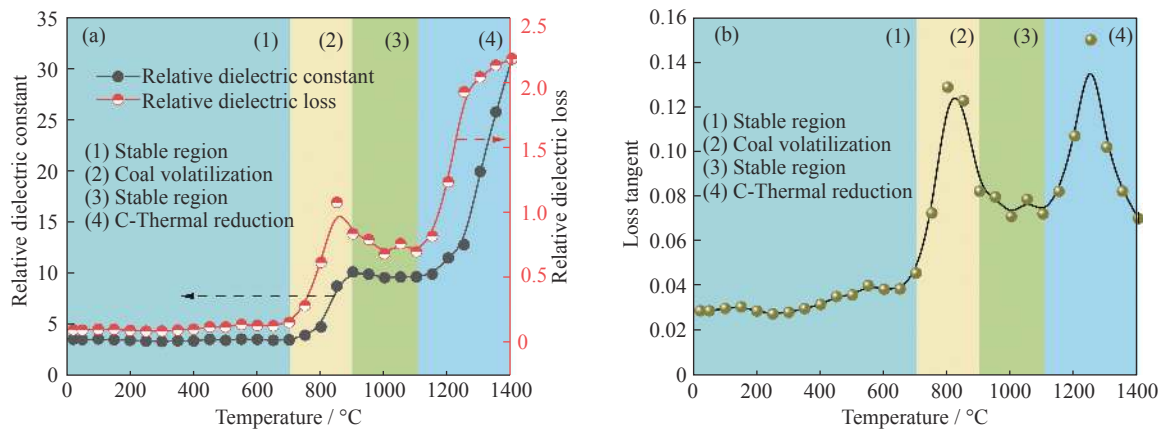


Fig. 6. (a) Relative dielectric constant and dielectric loss and (b) loss tangent of Ti-bearing blast furnace slag/pulverized coal mix as a function of temperature.

dielectric parameters tended to be stable. At the second critical point (1100°C), a large-scale reaction, related to carbo-thermal reduction, occurred, causing another increase in dielectric parameters. In addition, the change of the real part (relative dielectric constant) lagged behind that of the imaginary part (relative dielectric loss), and the higher the temperature, the more significant the lag effect. According to the change trend of the real part, the dielectric parameters–reaction temperature link can be divided into four regions (Fig. 6).

The reason about the real part changing lagged behind that of the imaginary part can be analyzed from the view of transient dipoles (TiO/TiO₂), which is caused by the bond breaking (stage I)–intermediate (stage II)–bonding (TiC, stage III) process, as shown in Fig. 7(a). Before the reaction, because of the stable atomic structure of the crystal, the microwave thermal effect was mainly due to the conduction loss, while the damping vibration loss of the dipoles was low. With the increase in temperature, after the original bond broke at the reaction interface, an intermediate state substance occurred, and the reaction product was generated rapidly; thus, the intermediate state substance featured transient dipoles.

For carbon [29], its unique delocalized π bond will undergo electron displacement polarization in large scale and even electrically conduct when interacting with microwaves, thus forming a delocalized polarized dipole. The presence of the dipole at the reaction interface will produce a traction effect on the surrounding transient dipoles (TiO/TiO₂), which is beneficial to the reaction. This traction is the M-NTE of microwaves acting on the reactions.

At the beginning of the reaction, the polarization intensity of molecules increased after bond breaking, but the intermediates were unstable and could not exist in large quantities, which led to the appearance and disappearance of intermediates, and once the intermediates appeared, the imaginary part increased. The main trend is that if the intermediate exists, it will contribute more damping loss to the interaction between the time-varying electromagnetic field and the sample, thus

increasing the dielectric loss. However, the intermediates disappeared in a very short time, could not form polarization equilibrium (orientation polarization), and could not contribute to the increase of the real part. Only when the reaction is stable and a large number of intermediates exist would the real part be changed by the intermediates, which would make the increase trend of the real part lag behind. In the later stage of the reaction, the rapid reduction of intermediates would also have a greater impact on the change of the imaginary part, which is the reason the peak of imaginary part occurred at 850°C (Fig. 6(a)).

The transient dipole phenomenon is the result of the interaction between the microwave and the crystalline structure material (TiO₂). The intensity of this phenomenon will affect the dielectric parameters; the higher the reaction rate, the stronger the phenomenon will be; in this way, the reaction was related to the dielectric parameters. Moreover, the promotion effect of the transient dipole phenomenon on the reaction process needs to be analyzed in combination with the delocalized polarization phenomenon of the carbon at the reaction interface. Because of the multi-atomic participation, the scale and intensity of the delocalization polarization of carbon were larger than those of the transient dipole phenomenon. In the time-varying microwave field, the local dipole orientation of the transient dipoles had a tendency to converge with the carbon delocalization polarization, which subjected the transient dipoles (TiO/TiO₂) generated at the reaction interface to the traction of the large π -bond delocalized polarized dipole of carbon, resulting in three effects: (1) a conducive separation of the intermediate (TiO/TiO₂) from the TiO₂ crystal body, reducing the probability of old bond formation; (2) a decrease in the distance of dipoles (TiO/TiO₂) to the carbon atoms and an increase in the probability of the contact between intermediates and carbon atoms; (3) an adjustment in the bonding angle of the intermediates (TiO/TiO₂) to increase the probability of bonding with carbon atoms.

Figs. 7(b) and 7(d) show the morphology of the TiC product and the recrystallized TiO₂ at the reaction interface caused by the traction effect, confirming the existence of M-NTE during microwave heating. Figs. 7(c) and 7(e) show that the iron present in the high-titanium slag participates in the microwave synthesis reaction of titanium carbide and is finally reduced to Fe metal and form a solid solution with TiC.

The presence of a small amount of iron in the product allows for the magnetic separation of TiC. Fig. 8 shows a suggested process flow chart of the microwave carbothermal synthesis of TiC from blast furnace slag and introduces the application direction of dielectric measurement.

Fig. 9 shows the XRD patterns of the main phase transformation during the reactions of the mixture sample subjected to microwave heating at different temperatures. New slag phases started to form at 900°C; the target material, TiC, started to form at 1150°C; when the temperature was 1200°C, within 30 min, the titanium oxide phase was almost com-

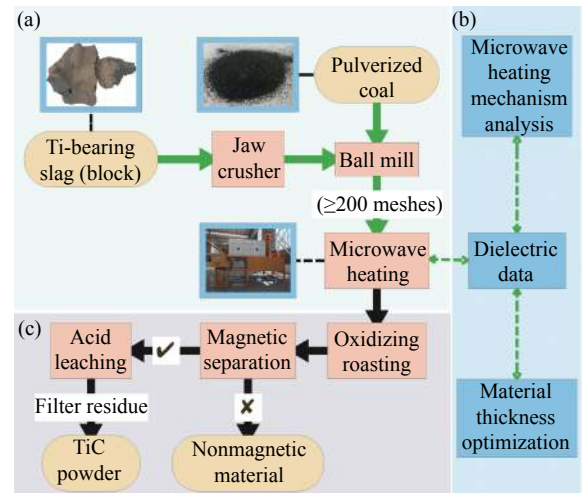


Fig. 8. (a) Flow charts of titanium carbide prepared by microwave heating from Ti-bearing blast furnace slag; (b) corresponding dielectric parameter applications; (c) work to be done.

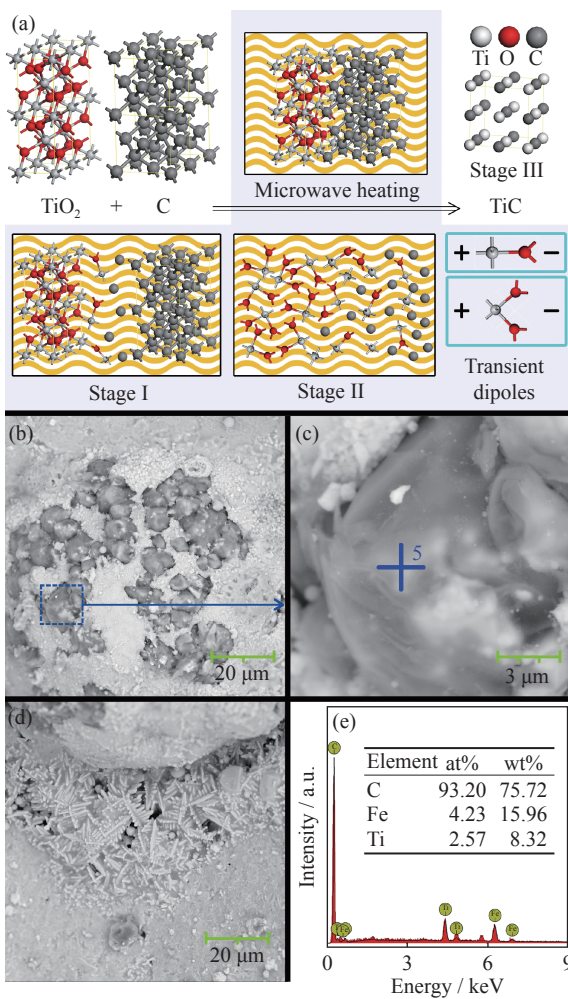


Fig. 7. (a) Mechanisms of dielectric phenomena; (b–d) SEM micrographs in the chemical reaction of titanium carbide synthesized by microwave heating (1200°C); (e) EDS analysis for point 5 in (c).

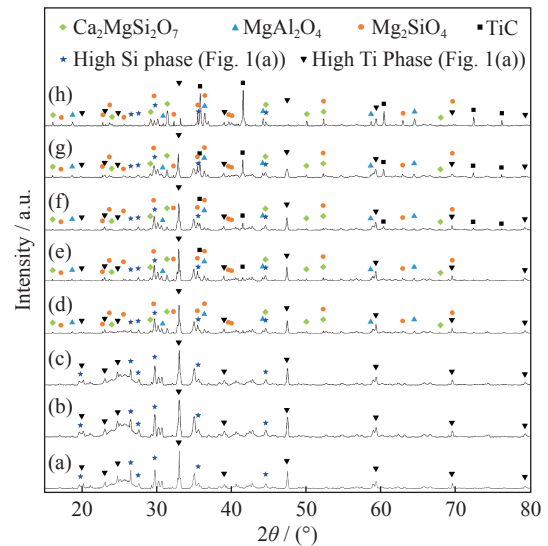


Fig. 9. XRD patterns of the mixture sample at different temperatures by microwave heating with microwave frequency of 2450 MHz: (a) 25°C; (b) 500°C, 5 min; (c) 700°C, 5 min; (d) 900°C, 5 min; (e) 1100°C, 5 min; (f) 1150°C, 5 min; (g) 1200°C, 5 min; (h) 1200°C, 30 min.

pletely transformed into titanium carbide. Iron was not detected as its amount was too small.

Fig. 10 shows that the reactions by microwave heating involved three steps: first, the slag phase started to float at 900°C; second, a higher degree of freedom for titanium oxide dendrites was obtained at 1100°C; finally, a large-scale titanium carbide synthesis occurred at 1200°C.

3.2. Thickness optimization

In a microwave reactor, the heating power of dielectric loss per unit volume determined by electric field distribution is given in Eq. (5) [30]:

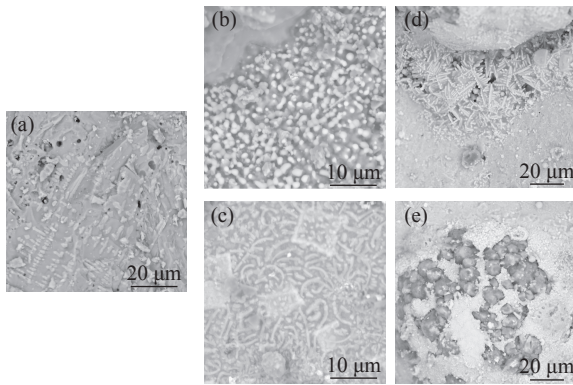


Fig. 10. Reaction course described by SEM at different critical temperatures: (a) room temperature; (b) 900°C; (c) 1100°C; (d, e) 1200°C.

$$\frac{dP_d}{dV_s} = \frac{1}{2} (2\pi f \varepsilon_0 \varepsilon_r'' \mathbf{E}^* \cdot \mathbf{E}) = \frac{1}{2} (2\pi f \varepsilon_0 \varepsilon_r' \tan \delta \cdot \mathbf{E}^* \cdot \mathbf{E}) = 2\pi f w \tan \delta \quad (5)$$

where P_d is the heating power caused by dielectric loss, V_s is the volume of the sample, f is the microwave frequency (2450 MHz), \mathbf{E} is the intensity of external electric field, \mathbf{E}^* is the complex conjugation of \mathbf{E} , and w is the *in situ* energy storage power of materials (unit volume) shown in Eq. (6).

$$w = \frac{1}{2} \varepsilon_0 \varepsilon_r' \mathbf{E}^* \cdot \mathbf{E} \quad (6)$$

Eq. (5) shows that the heating power of the dielectric loss per unit volume of material is related to the *in situ* storage power and loss tangent, while the *in situ* storage power is related to the relative dielectric constant and the *in situ* electric field intensity. The *in situ* electric field intensity is related to the initial microwave power (P_0), and the increase in material thickness will also change the electric field intensity distribution in the region where the material is located. Therefore, the analysis of microwave energy utilization efficiency η_{M2} (Eq. (7)) should consider both the material quantity (material thickness) and the initial power P_0 in the microwave heating cavity. In this paper, the relationship between the microwave utilization efficiency and the material thickness is discussed from the perspectives of penetration depth and reflection loss under the condition of the power guaranteeing material heating rate.

$$\eta_{M2} = \frac{P_d}{P_0} \quad (7)$$

In the microwave heating process, the material is usually loaded in a transmissive container to a certain thickness and placed at the bottom of the metal cavity. In this way, the phenomena of penetration and reflection will inevitably occur in the interaction process between the materials and microwave. By measuring the dynamic dielectric parameters of Ti-bearing blast furnace slag/pulverized coal at a high temperature and combining the analysis methods of penetration depth and

reflection loss, the optimum thickness range of the material during microwave heating can be deduced.

3.2.1. Thickness optimization by penetration depth

Electromagnetic waves propagating in dielectric materials can cause energy attenuation. Materials with different dielectric properties also feature different attenuation effects. When the energy of electromagnetic wave attenuates to $1/e$ (natural constant $e \approx 2.718281828$) of the energy before incidence (E_0), that is $E_{D_p} = E_0/e$, the corresponding depth of transmission in materials is D_p [31]. The penetration depth (D_p) describes the absorbing properties of dielectric materials from the viewpoint of energy attenuation during electromagnetic wave propagation in dielectric materials, and can be calculated using dielectric parameters according to Eq. (8):

$$D_p = \frac{c}{2\sqrt{2}f\pi\sqrt{\varepsilon_r' \left[\sqrt{1 + \left(\frac{\varepsilon_r''}{\varepsilon_r'}\right)^2} - 1 \right]}} \quad (8)$$

where c is the speed of light in free space ($3 \times 10^8 \text{ m}\cdot\text{s}^{-1}$). The calculation results of penetration depth as a function of temperature ($D_p(T)$) are shown in Fig. 11. The polynomial fitting results are described by Eq. (9):

$$D_p(T) = 5.7236 \times 10^{-10} T^3 - 1.1779 \times 10^{-6} T^2 + 3.4393 \times 10^{-4} T + 0.3302 \quad (9)$$

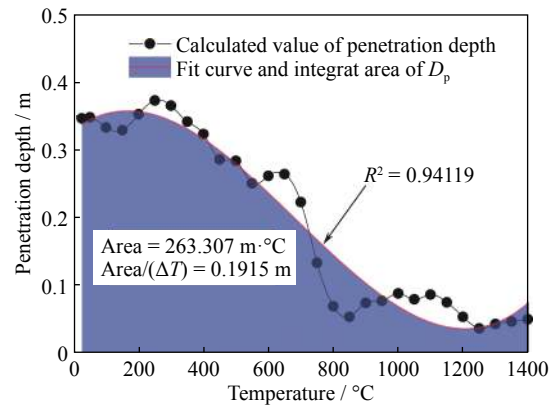


Fig. 11. Penetration depth of the Ti-bearing blast furnace slag/pulverized coal as a function of temperature ($\Delta T = (1400 - 25)^\circ\text{C} = 1375^\circ\text{C}$).

The fitting degree ($R^2 = 0.94119$) is close to 1, which indicates that the fitting function could clearly describe the changing trend and integral of the penetration depth. For the microwave heating process, the temperature and penetration depth are variable. To optimize thickness, the average penetration depth (\bar{D}_p) should be introduced (Eq. (10)):

$$\bar{D}_p = \frac{1}{T - T_0} \int_{T_0}^T D_p(T) dT \quad (10)$$

where T_0 is the initial temperature to calculate \bar{D}_p .

In this work, the average penetration depth of the whole integral interval (25–1400°C), $\bar{D}_p|_{25}^{1400}$, is determined by Eqs.

(9) and (10), and the value is 0.1915 m. This value can be used as the upper limit of the thickness optimization interval. For the microwave heating process, because the reaction occurs in the high-temperature stage, to make the reaction proceed smoothly, setting excessive material thickness is not appropriate; therefore, the average penetration depth of the second half of the heating process (700–1400°C), $\bar{D}_p|_{700}^{1400}$, can be set as the lower limit of the thickness optimization interval ($\bar{D}_p|_{700}^{1400} = 0.0808$ m). In this way, under appropriate power conditions, the optimum range of material thickness determined by penetration depth is 0.0808–0.1915 m.

If the material thickness is below this range, although the heating effect can be improved, the microwave utilization efficiency of the material will be reduced. In fact, when the material thickness is reduced, the microwave penetrating the material will carry more energy and have a greater probability of non-heating loss outside the material area.

3.2.2. Thickness optimization by reflection loss

The cavity of the microwave heating equipment is designed to be a metal plate wall, because the metal plate can completely reflect electromagnetic wave in theory. When a certain thickness of material is laid flat on a metal plate and the electromagnetic wave is incident vertically, a part of the electromagnetic wave will be reflected back. The relationship between the reflection power and the incident power can be described by the reflection loss (RL) under this condition. That is, the reflection loss describes the material absorbance performance from the viewpoint of energy loss in the electromagnetic wave reflection process. Based on the transmission line theory [32], the reflection loss parameters can be deduced according to Eq. (11).

$$RL = 20 \lg \frac{\left| \sqrt{\frac{\mu_r}{\epsilon_r}} \tan h \left(i \frac{2\pi f}{c} \sqrt{\mu_r \epsilon_r} d \right) - 1 \right|}{\left| \sqrt{\frac{\mu_r}{\epsilon_r}} \tan h \left(i \frac{2\pi f}{c} \sqrt{\mu_r \epsilon_r} d \right) + 1 \right|} \quad (11)$$

where μ_r is relative permeability and is assumed to be 1 in the RL calculation, $\tan h$ is hyperbolic tangent function, and d is the thickness of the materials loaded on the metallic plate.

The reflection loss of the mixture sample at different temperatures can be calculated by taking the relative dielectric parameters into Eq. (11). Fig. 12 shows the relationship between the reflection loss (RL) and material thickness. The thickness optimization based on reflection loss can be realized by determining the material thickness corresponding to the three RL values of -10 dB ($\eta_{M2} = 90\%$), -20 dB ($\eta_{M2} = 99\%$), and the minimum of reflection loss (RL_{\min} , $\eta_{M2} > 99\%$) in Fig. 12 at different temperatures. Taking the determination of thickness at 400, 800, 1000, and 1400°C as an example, the material thicknesses determined by RL values of -10 dB, -20 dB, and RL_{\min} are d_1 , d_2 and d_{peak} , respectively. The material thickness determined under other temperatures is shown in Table 5.

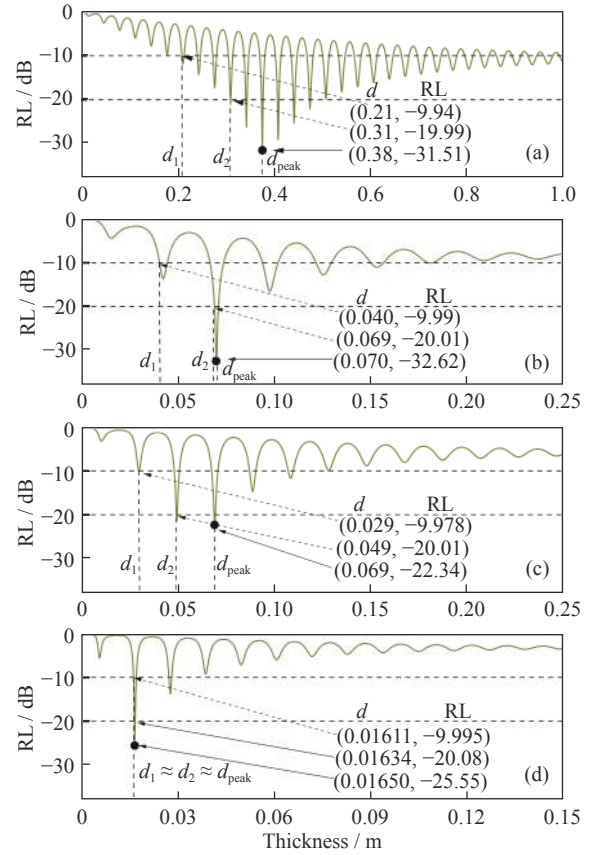


Fig. 12. RL of Ti-bearing blast furnace slag/pulverized coal as a function of thickness at different temperatures: (a) 400°C; (b) 800°C; (c) 1000°C; (d) 1400°C.

In this work, three selected reflective loss values (-10 dB, -20 dB, and RL_{\min}) were used to determine the global average depth and the high-temperature average depth, as shown in Table 6. The reflection loss can be used to determine three thickness ranges with three different η_{M2} , in which the upper limits of \bar{d}_1 (RL of -10 dB, η_{M2} of 90%), \bar{d}_2 (RL of -20 dB, η_{M2} of 99%), and \bar{d}_{peak} (RL_{\min} , η_{M2} of >99%) are the global average material thickness (average values of d_1 , d_2 , and d_{peak} calculated at 25–1400°C in Table 5), determined by a different microwave energy utilization efficiency, and the lower limits of \bar{d}_1 (RL of -10 dB, η_{M2} of 90%), \bar{d}_2 (RL of -20 dB, η_{M2} of 99%), and \bar{d}_{peak} (RL_{\min} , η_{M2} of >99%), similar to that determined using the penetration depth optimization method above, are the average thickness of the high-temperature (700–1400°C) section (average values of d_1 , d_2 , and d_{peak} calculated at 700–1400°C in Table 5). From Table 6, under the condition of the power guaranteeing the material heating rate, the closer the material thickness range of the actual heating is to the upper limit of material thickness optimum range determined by penetration depth (0.0808–0.1915 m), the greater is the microwave energy utilization efficiency. Usually the microwave heating equipment operates at low power under laboratory conditions; therefore, this study is more suitable

Table 5. Thickness confirmation by selected RL values

Temperature / °C	d_1 / m	d_2 / m	d_{peak} / m	RL _{min} / dB
25	0.2076	0.3359	0.4010	-35.3647
50	0.2076	0.3372	0.4030	-47.4313
100	0.2062	0.3039	0.4000	-33.9392
150	0.2082	0.3064	0.3715	-35.8814
200	0.2107	0.3414	0.4075	-35.2066
250	0.2141	0.3777	0.4445	-50.3305
300	0.2142	0.3472	0.4465	-44.6715
350	0.2112	0.3429	0.4095	-40.1304
400	0.2113	0.3113	0.3775	-31.5085
450	0.1750	0.2724	0.3375	-39.7087
500	0.1775	0.2761	0.3420	-42.8506
550	0.1435	0.2396	0.3045	-34.6451
600	0.1745	0.2409	0.3055	-39.4536
650	0.1768	0.2756	0.3095	-40.9807
700	0.1438	0.2099	0.2750	-32.0903
750	0.0754	0.1364	0.1375	-32.7202
800	0.0403	0.0687	0.0698	-32.6206
850	0.0297	0.0308	0.0311	-21.3671
900	0.0282	0.0476	0.0480	-52.2099
950	0.0286	0.0481	0.0485	-33.8752
1000	0.0296	0.06387	0.0691	-22.3966
1050	0.0290	0.0487	0.0492	-30.2159
1100	0.0293	0.0489	0.0491	-22.9615
1150	0.0285	0.0481	0.0485	-47.1966
1200	0.0261	0.0269	0.0271	-21.5858
1250	0.0245	0.0256	0.0256	-20.0026
1300	0.0199	0.0204	0.0206	-30.1015
1350	0.0176	0.0179	0.0181	-38.3773
1400	0.0161	0.0164	0.0165	-25.5536

Table 6. Thickness optimization comparison between the results of RL and penetration depth (\bar{D}_p) methods

Limit	Calculated temperature range / °C	RL method			Penetration depth method
		\bar{d}_1 / m	\bar{d}_2 / m	\bar{d}_{peak} / m	\bar{D}_p / m
Lower limit	700–1400	0.0378	0.0572	0.0622	0.0808
Upper limit	25–1400	0.1140	0.1782	0.2136	0.1915

for the design of large-scale industrial microwave heating reactors.

4. Conclusion

Microwave carbothermal synthesis of blast furnace slag is an important application of microwave heating technology in solid waste resource recovery. In this study, the reaction mechanism was analyzed using dielectric parameters. During the chemical reaction of microwave carbothermal synthesis of titanium carbide from blast furnace slag, the transient dipole polarization phenomenon appearing at the reac-

tion interface had a significant effect on the dielectric parameters. Meanwhile, a large π bond caused by the presence of multiple carbon atoms at the reaction interface resulted in a delocalization displacement polarization phenomenon. Two polarization phenomena existing in the microwave field can promote the titanium carbide synthesis reaction, which is the embodiment of microwave macroscopic non-thermal effect. The SEM results of the sample during the reaction showed the recrystallization of the enriched titanium oxide; this confirms the dipoles traction caused by the macroscopic non-thermal effect. Moreover, the XRD patterns at different temperatures confirm the phase transformation in the reactions. The material thickness was optimized to obtain a high energy efficiency. The results show that the optimum range of material thickness determined by RL_{min} ($\eta_{M2} > 99\%$) is basically the same as that determined by penetration depth analysis (0.0808–0.1915 m). The optimum range of material thickness plays an important role in the design of microwave heating reactor for treating Ti-bearing blast furnace slag.

Acknowledgements

This work was financially supported by the National Key R&D Program of China (No. 2018YFC1900500), the National Natural Science Foundation of China (No. 51961020), the Key Technology Research and Industrialization Application Demonstration Project of the Renewable Multi-energy Complementary (No. 2018IB020), and the Academician Workstation of Kefa Cen (No. 2018IC085).

References

- [1] Y.Z. Wang, J.L. Zhang, Z.J. Liu, and C.B. Du, Carbothermic reduction reactions at the metal-slag interface in Ti-bearing slag from a blast furnace, *JOM*, 69(2017), No. 11, p. 2397.
- [2] J.X. Liu, G.J. Cheng, Z.G. Liu, M.S. Chu, and X.X. Xue, Reduction process of pellet containing high chromic vanadium-titanium magnetite in cohesive zone, *Steel Res. Int.*, 86(2015), No. 7, p. 808.
- [3] S. Wang, Y.F. Guo, T. Jiang, L. Yang, F. Chen, F.Q. Zheng, X.L. Xie, and M.J. Tang, Reduction behaviors of iron, vanadium and titanium oxides in smelting of vanadium titanomagnetite metallized pellets, *JOM*, 69(2017), No. 9, p. 1646.
- [4] S. Wang, M. Chen, Y.F. Guo, T. Jiang, and B.J. Zhao, Reduction and smelting of vanadium titanomagnetite metallized pellets, *JOM*, 71(2019), No. 3, p. 1144.
- [5] Y.M. Zhang, L.N. Wang, D.S. Chen, W.J. Wang, Y.H. Liu, H.X. Zhao, and T. Qi, A method for recovery of iron, titanium, and vanadium from vanadium-bearing titanomagnetite, *Int. J. Miner. Metall. Mater.*, 25(2018), No. 2, p. 131.
- [6] M. Zhou, T. Jiang, S.T. Yang, and X.X. Xue, Vanadium-titanium magnetite ore blend optimization for sinter strength based on iron ore basic sintering characteristics, *Int. J. Miner. Process.*, 142(2015), p. 125.
- [7] C. Lv, K. Yang, S.M. Wen, S.J. Bai, and Q.C. Feng, A new technique for preparation of high-grade titanium slag from ti-

- tanomagnetite concentrate by reduction–melting–magnetic separation processing, *JOM*, 69(2017), No. 10, p. 1801.
- [8] H.H. Lü, M.Z. Wu, Z.L. Zhang, X.R. Wu, L.S. Li, and Z.F. Gao, Co-precipitation behaviour of titanium-containing silicate solution, *Chem. Pap.*, 70(2016), No. 12, p. 1632.
- [9] Y.J. Zhang, T. Qi, and Y. Zhang, A novel preparation of titanium dioxide from titanium slag, *Hydrometallurgy*, 96(2009), No. 1-2, p. 52.
- [10] Y.F. Guo, S.S. Li, T. Jiang, G.Z. Qiu, and F. Chen, A process for producing synthetic rutile from Panzhihua titanium slag, *Hydrometallurgy*, 147-148(2014), p. 134.
- [11] D. Wang, J.L. Chu, J. Li, T. Qi, and W.J. Wang, Anti-caking in the production of titanium dioxide using low-grade titanium slag via the NaOH molten salt method, *Powder Technol.*, 232(2012), p. 99.
- [12] T. Jiang, X.X. Xue, P.N. Duan, X. Liu, S.H. Zhang, and R. Liu, Carbothermal reduction–nitridation of titania-bearing blast furnace slag, *Ceram. Int.*, 34(2008), No. 7, p. 1643.
- [13] G. Chen, J. Chen, and J.H. Peng, Effects of mechanical activation on structural and microwave absorbing characteristics of high titanium slag, *Powder Technol.*, 286(2015), p. 218.
- [14] C.B. Cheng, R.H. Fan, Z.Y. Wang, Q. Shao, X.K. Guo, P.T. Xie, Y.S. Yin, Y.L. Zhang, L.Q. An, Y.H. Lei, J.E. Ryu, A. Shankar, and Z.H. Guo, Tunable and weakly negative permittivity in carbon/silicon nitride composites with different carbonizing temperatures, *Carbon*, 125(2017), p. 103.
- [15] T. Ono and M. Ueki, Effect of graphite addition on the microstructure and mechanical properties of hot-pressed titanium carbide, [in] S. Somiya, ed., *Advanced Materials '93. Ceramics, Powders, Corrosion and Advanced Processing*, Elsevier, Amsterdam, Netherlands, 1994, p. 585.
- [16] A.M. Shul'pekov and G.V. Lyamina, Electrical and thermo-mechanical properties of materials based on nonstoichiometric titanium carbide prepared by self-propagating high-temperature synthesis, *Inorg. Mater.*, 47(2011), No. 7, p. 722.
- [17] L. Pan, T. Shoji, A. Nagataki, and Y. Nakayama, Field emission properties of titanium carbide coated carbon nanotube arrays, *Adv. Eng. Mater.*, 9(2007), No. 7, p. 584.
- [18] Z.W. Peng, J.Y. Hwang, B.G. Kim, J. Mouris, and R. Hutcheon, Microwave absorption capability of high volatile bituminous coal during pyrolysis, *Energy Fuels*, 26(2012), No. 8, p. 5146.
- [19] G.B. Dudley, R. Richert, and A.E. Stigman, On the existence of and mechanism for microwave-specific reaction rate enhancement, *Chem. Sci.*, 6(2015), No. 4, p. 2144.
- [20] M. Damm and C.O. Kappe, Parallel microwave chemistry in silicon carbide reactor platforms: An in-depth investigation into heating characteristics, *Mol. Diversity*, 13(2009), No. 4, p. 529.
- [21] C.A. Kuhn, E.L. Dall'Oglio, and P.T. de Sousa, Quantum tunneling contribution for the activation energy in microwave-induced reactions, *J. Phys. Chem. A*, 121(2017), No. 30, p. 5735.
- [22] S.H. Li, C. Akyel, and R.G. Bosisio, Precise calculations and measurements on the complex dielectric constant of lossy materials using TM₀₁₀ cavity perturbation techniques, *IEEE Trans. Microwave Theory Tech.*, 29(1981), No. 10, p. 1041.
- [23] Y.P. Zhang, E. Li, J. Zhang, C.Y. Yu, H. Zheng, and G.F. Guo, A broadband variable-temperature test system for complex permittivity measurements of solid and powder materials, *Rev. Sci. Instrum.*, 89(2018), No. 2, art. No. 024701.
- [24] *Dielectric Constant* [2010-12-14]. http://www.vias.org/encyclopedia/phys_dielectric_const.htm
- [25] R. Buchner, J. Barthel, and J. Stauber, The dielectric relaxation of water between 0°C and 35°C, *Chem. Phys. Lett.*, 306(1999), No. 1-2, p. 57.
- [26] T. Meissner and F.J. Wentz, The complex dielectric constant of pure and sea water from microwave satellite observations, *IEEE Trans. Geosci. Remote Sens.*, 42(2004), No. 9, p. 1836.
- [27] J.W. Chen, Y. Jiao, and X.D. Wang, Thermodynamic studies on gas-based reduction of vanadium titano-magnetite pellets, *Int. J. Miner. Metall. Mater.*, 26(2019), No. 7, p. 822.
- [28] Z.W. Peng, X.L. Lin, Z.Y. Li, J.Y. Hwang, B.G. Kim, Y.B. Zhang, G.H. Li, and T. Jiang, Dielectric characterization of Indonesian low-rank coal for microwave processing, *Fuel Process. Technol.*, 156(2017), p. 171.
- [29] D. Beneroso, A. Albero-Ortiz, J. Monzó-Cabrera, A. Díaz-Morcillo, A. Arenillas, and J.A. Menéndez, Dielectric characterization of biodegradable wastes during pyrolysis, *Fuel*, 172(2016), p. 146.
- [30] X.L. Zhang, D.O. Hayward, and D.M.P. Mingos, Microwave dielectric heating behavior of supported MoS₂ and Pt catalysts, *Ind. Eng. Chem. Res.*, 40(2001), No. 13, p. 2810.
- [31] R. Meredith, *Engineers' Handbook of Industrial Microwave Heating*, The Institution of Engineering and Technology, London, 1998.
- [32] D.M. Pozar, *Microwave Engineering*, 4th ed., John Wiley & Sons, Inc., New York, 2011.